Trajectory and vibration control of 2-link flexible manipulator using inversion control system

Daiki Maeno [1], Minoru Sasaki [2,*], Joseph Muguro [3], Waweru Njeri [3], Jackline Asango [3], Titus Mulembo [3], and Kojiro Matsushita [1,2]

[1]*Gifu University (Department of Mechanical Engineering, 501-1121, 1-1 Yanagido, Gifu, Japan).*

[2]*Intelligent Production Technology Research & Development Center for Aerospase (IPTeCA).*

[3]*Dedan Kimathi University of Technology (School of Engineering).*

[*]*Corresponding Author - Email: sasaki.minoru.n3@f.gifu-u.ac.jp; 501-1121, 1-1 Yanagido; Tel.: (+81-58-293-2541).*

Abstract Flexible manipulators capable of high speed operations with low energy consumption have high potential uses for large-scale deployment in industrial works. However, for such systems, simultaneous control of trajectory and vibration still remains a challenge. This paper describes the development of a controller that enables trajectory and vibration control. The controller performance was tested and verified through simulations and actual experiments with a laboratory grade 3D 2-link, flexible manipulator. As a baseline, trajectory tracking using inverse kinematics was observed to have poor tracking due to self-weight deflection. Inverse kinematics results was used to acquire a model of the manipulator using canonical variate analysis system identification. Further, an inverse system was modeled for simultaneous trajectory and vibration control. Compared against the inverse kinematic and the traditional direct strain feedback (DSFB) controller, the inverse system model was found to have 9-fold decrease in trajectory error tracking as well as vibration suppression. The validation experiments on the actual manipulator showed that the inverse system based controller was superior to the inverse kinematics and DSFB method of tracking as it followed the ideal trajectory by overcoming the gravitational pull, and suppressed the link vibrations.

Keywords Flexible Manipulator, Mechanics, Vibration control, Inverse system

1. Introduction

Currently, industrial robot arms are required to have low cost, low energy consumption, high accuracy, and high speeds of operations. This are competing requirements as far as construction of the manipulator arms goes since heavy and bulky robot arm construction can increase repeatability and precision while lowering the operating speeds. Additionally, bulky arms require more energy to operate. One of the potential solutions is to reduce links weight. In this case, weight reduction of the arm leads to lower rigidity of the arm. Switching from rigid to flexible links have been shown to simplify the mechanical design and save energy while achieving higher speeds of operations which inevitable leads to improved system performance [1]–[3]. On the other hand, the accuracy of the tip position is reduced by vibration due to elastic deformation, so the construction of a controller for

vibration suppression becomes a necessity [4], [5].

As noted above, the construction of manipulator is an important aspect of the robot arm. Source of vibration in robots can be categorized into two, joint and link flexibility [6]. In joint flexibility, the motion transmission elements e.g., harmonic drives, belts, etc., of the robot flex during operation. Link flexibility on the other hand is brought about by the construction of the link. Figure 1 outlines the difference between flexible and rigid link as considered in this paper. From literature review, the one-link arm is called a flexible arm whereas the two-link or more arm is called a flexible manipulator.

Most of the studies we found focused on a single-link flexible arm with few articles on multi-link manipulator. In addition, owing to the construction of the link, most of the inquiry has been focused on vibration suppression [7]–[10]. Authors in [11]–[13] proposed the direct strain feedback for vibration control. This scheme
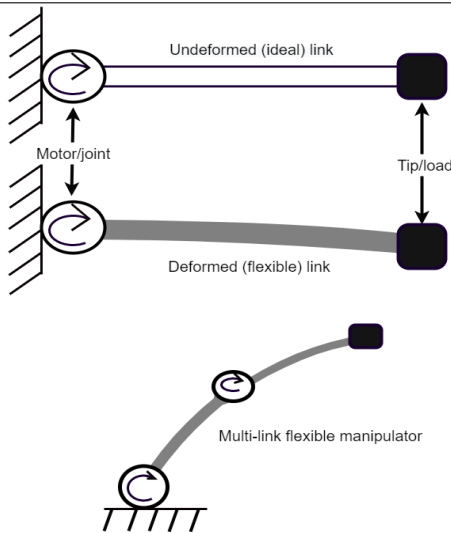
Fig. 1. Structural illustration of multi-link manipulator

(a) Actual manipulator

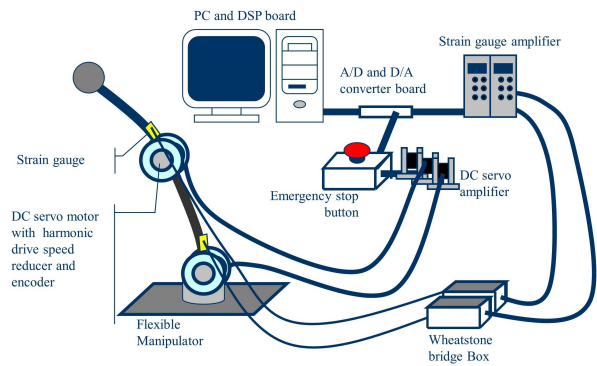(b) Control system of the manipulator

Fig. 2. Flexible manipulator

involves feeding back a fraction of root strain through a controller gain k. In their work, they showed that strain feedback has the effect of increasing the system damping thereby reducing vibrations and has no effect on the system stiffness. They further presented a proof that the scheme is asymptotically stable. Fixed controllers are limited in that they allow noise feedback once the strain has subsided. Adaptive controller gain is proposed in [14], [15] with better results that those of fixed gains.

Researchers in [16] proposed an energy based robust controller for a multi-link flexible robot. In their work, the controller is developed from the basic relationship of energy, and it is independent from system dynamics. This approach has the advantage in that the derivation of the system model, which is very difficult for a multi-link manipulator, is not required. Other techniques in literature includes but not limited to robust control [17], input shaping [18] to mention just but a few.

Trajectory tracking is also a significant in multi-link manipulators. We found few studies on trajectory control of the tip of a multi-link manipulator with most inquiries directed towards single link. Flexible manipulators have more complicated kinematic and dynamic equations than rigid manipulators, and deformation must be taken into account. Many nonlinear elements such as higher-order modes, longitudinal deformation, nonlinear friction torque, and other nonlinear variables must be considered simultaneously in order to adequately characterize the flexible manipulators [19]. There are numerous nonlinear components in the dynamic equations of the flexible manipulator system when all of these nonlinear elements are taken into account. This leads to complex computation that impact real-time control. These issues necessities simplification of the manipulator model. The simplification has to properly considered. If the nonlinear factors are ignored, the model is unusable as uncertainties increases. Several research have been conducted towards this problem.
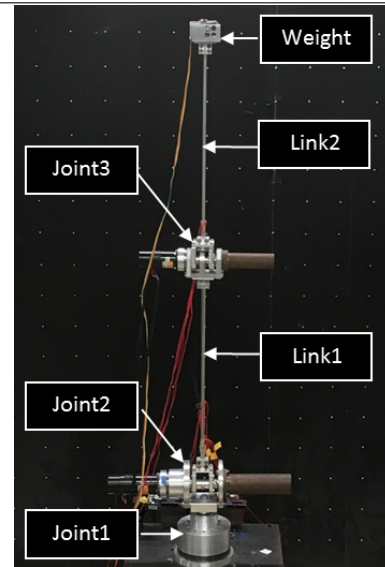
Approaches like kinematic model, linearization about the equilibrium point via the Jacobian method, and feedback linearization have been proposed for stabilization and trajectory tracking [6], [7], [20], [21]. The Jacobian method is limited as it neglects the nonlinearities while operating around the equilibrium point. In kinematic model, the Devavit-Hartenberg (DH) convention is the most popular. Similar to the linearization model, the DH convention fails to capture all the nonlinear dynamics of a flexible manipulator as discussed in [6], [22].

The other alternative is feedback linearization which handles the nonlinearities by changing the variables instead of neglecting them. Other approaches include but not limited to mode decomposition, neuro-fuzzy modeling, machine learning approaches, Kalman filters among others [8], [19], [23]–[25].

The current paper utilized system identification to generate a model and applied system inversion to suppression vibration as well as achieve trajectory planning. The performance of the proposed scheme is compared to that of a feedback scheme and a DH model for reference. In this research, we ignore link flexion and utilize forward

and inverse kinematics to express the tip trajectory in terms of the joint trajectories as if the robot were comprised of rigid links. Next, using the input-output data obtained, system identification of the flexible manipulator was performed by the subspace identification method, and an inverse system for the purpose of tip trajectory control was developed. Finally, for verification of the inverse system, the performance of the controller was tested using a laboratory-grade actual manipulator.

2. Experimental setup

Figure 2 shows a flexible manipulator with two links and three degrees of freedom. A motor is attached to each joint with Joint 2 and joint 3 rotating in the elevation direction while joint 1 is rotating in the twisting direction giving the manipulator a 3D sweep. A cast iron cylinder is mounted on the opposite side of each motor to keep the arms balanced. Each motor also has a built-in optical encoder with output of 1000 *pulses/rev*. Link 1 uses stainless steel (SUS304) and link 2 uses aluminum (A2017).

In order to measure elastic and torsional deformation, strain gauges are attached to the roots of Link 1 and Link 2 in the rotation directions of Joint 2 and Joint 3 and twisting direction of joint 1 respectively using the 2-gauge method. The strain signal is conditioned using a bridge circuit before being amplified using DPM713B and DPM913B strain amplifiers(DPM713B and DPM913B made by Kyowa Electric Co. Ltd.). These amplified signals are sampled at 0.01sec and digitized with an ADC interface to dSPACE™DSP board for management. The physical model is shown in Figure 2(a) while the basic representation of the control system is shown in Figure 2(b).

A weight is attached to the tip of the second link of the manipulator which makes the link easily deformed during operation. The control system comprises of Matlab/Simulink™from where the desired trajectory is synthesized and the control system layout designed. The Simulink model is downloaded to dSPACE Control desk which interfaces the hardware parts of the system collects feedback signals for display and further processing.

The output signal is sent to the speed control type servo amplifier (DA2 series by Sanyo Denki) through the D/A converter to drive the servo motor. In this experiment, P controller is chosen for the joint angle control. The reason is that I controller would cause overshoot or undershoot, which in turn would result in severe link vibrations. Further, D controller would cause oscillations in the angular response, and as a result, would cause vibration of the entire link.

In this study, vibration control is one of the key objective, to this end, the proportional gain was chosen to equal to 3. The trajectory of the arm tip was captured using an optical motion capture (OptiTrack™) which tracks a lightweight marker attached to the tip in three-

Table 1. DH parameters of the manipulator

Link	$a_i[m]$	$\alpha_i[degree]$	$d_i[m]$	$\theta_i[degree]$
0	0	$\pi/2$	0	θ_1
1	0.569	l_2	0	θ_2
2	0.57	l_3	0	θ_3

dimensional space. For this experiment, the sampling cycle during measurement was set to 100 Hz. The vertical axis was chosen as the positive z axis, the horizontal left is the positive x axis, and the forward direction is the positive y axis.

3. Inverse kinematics control

In this paper, inverse kinematics was used to develop joint trajectories so that the tip of the manipulator would trace a circle having radius of 0.15m centered on a position of 0.8m in the y direction and 0.5m in the z direction with the base of the manipulator as the origin. The angular velocity of the circle at this time was chosen as 1.25rad/sec, slow enough for rigid manipulator assumption to hold.

Table 1 shows the Devavit-Hartenberg(DH) parameter of the flexible manipulator. The coordinate system set for each link is $\Sigma_i = \{x_i, y_i, z_i\}$, the rotation matrix $^{i-1}\mathbf{R}_i$ associated with the conversion from Σ_{i-1} to Σ_i and the position vector $^{i-1}\mathbf{d}_i$ are as shown in (1) - (6) as follows

$$^0R_1 = \begin{bmatrix} \cos\theta_1 & 0 & \sin\theta_1 \\ \sin\theta_1 & 0 & -\cos\theta_1 \\ 0 & 1 & 0 \end{bmatrix} \tag{1}$$

$$^1R_2 = \begin{bmatrix} \cos\theta_2 & 0 & -\sin\theta_2 \\ \sin\theta_2 & 0 & -\cos\theta_2 \\ 0 & 1 & 0 \end{bmatrix} \tag{2}$$

$$^2R_3 = \begin{bmatrix} \cos\theta_3 & 0 & -\sin\theta_3 \\ \sin\theta_3 & 0 & \cos\theta_3 \\ 0 & 1 & 0 \end{bmatrix} \tag{3}$$

$$^0d_1 = \begin{bmatrix} 0 \\ 0 \\ 0 \end{bmatrix} \tag{4}$$

$$^1d_2 = \begin{bmatrix} l_1\cos\theta_2 \\ l_1\sin\theta_2 \\ 0 \end{bmatrix} \tag{5}$$

$$^2d_3 = \begin{bmatrix} l_2\cos\theta_3 \\ l_2\sin\theta_3 \\ 0 \end{bmatrix} \tag{6}$$

The simultaneous conversion matrix $^{i-1}T_i$ from Σ_{i-1} to Σ_i is given by (7) as follows

$$^{i-1}T_i = \begin{bmatrix} R & d \\ 0 & 1 \end{bmatrix} \tag{7}$$

From this, the simultaneous conversion matrix between

each link is given by (8) - (10) for link 1-3, as follows.

$$^0T_1 = \begin{bmatrix} \cos\theta_1 & 0 & \sin\theta_1 & 0 \\ \sin\theta_1 & 0 & -\cos\theta_1 & 0 \\ 0 & 1 & 0 & 0 \\ 0 & 0 & 0 & 1 \end{bmatrix} \quad (8)$$

$$^1T_2 = \begin{bmatrix} \cos\theta_2 & 0 & -\sin\theta_2 & l_1\cos\theta_2 \\ \sin\theta_2 & 0 & -\cos\theta_2 & l_1\sin\theta_2 \\ 0 & 1 & 0 & 0 \\ 0 & 0 & 0 & 1 \end{bmatrix} \quad (9)$$

$$^2T_3 = \begin{bmatrix} \cos\theta_3 & 0 & -\sin\theta_3 & l_2\cos\theta_3 \\ \sin\theta_3 & 0 & \cos\theta_3 & l_2\sin\theta_3 \\ 0 & 1 & 0 & 0 \\ 0 & 0 & 0 & 1 \end{bmatrix} \quad (10)$$

Therefore, the transformation matrix from the reference coordinate system at the root to the coordinate system to the tip of the flexible manipulator is given by (11).

$$^0T_3 = {}^0T_1^1T_2^2T_3 \quad (11)$$
$$= \begin{bmatrix} ^0R_3 & ^0d_3 \\ 0 & 1 \end{bmatrix}$$

The expanded transformation matrix is attached in appendix A. The coordinates of the tip of the manipulator can be expressed as in (12).

$$^0d_3 = \begin{bmatrix} \cos\theta_1(l_1\cos\theta_2 + l_2\cos(\theta_2+\theta_3)) \\ \sin\theta_1(l_1\cos\theta_2 + l_2\cos(\theta_2+\theta_3)) \\ l_1\sin\theta_2 + l_2\sin(\theta_2+\theta_3) \end{bmatrix} \quad (12)$$

By solving equation (12), joint angle 1, 2 and 3 becomes (13) - (15).

$$\theta_1 = \operatorname{atan2}(y,x) \quad (13)$$

$$\theta_2 = \sin^{-1}\left(\frac{z}{\sqrt{l_1^2 + l_2^2 + 2l_1l_2\cos\theta_3}}\right) \quad (14)$$

$$\theta_3 = \cos^{-1}\left(\frac{x^2 + y^2 + z^2 - l_1^2 - l_2^2}{2l_1l_2}\right) \quad (15)$$

In this case, α satisfies the condition in (16).

$$\cos\alpha = \frac{l_1 + l_2\cos\theta_3}{\sqrt{l_1^2 + l_2^2 + 2l_1l_2\cos\theta_3}} \quad (16)$$

The results of the modeling are reported in Figure 3 for confirmation of performance. The figure shows the trajectory of the tip plotted against the desired tip trajectory. The reported deviations were -0.0067 [m] in the z direction and 0.0021 [m] in the y direction. The radius error was 0.0085 [m] in the z direction and -0.0016 [m] in the y direction, i.e, the error of the radius of the circle and the deviation of the center were less than 1cm, confirming the accuracy of the inverse kinematics above. The error generated here is considered to be caused by the change in the length of the link caused by the bending of the link due to its own weight. Further, performed
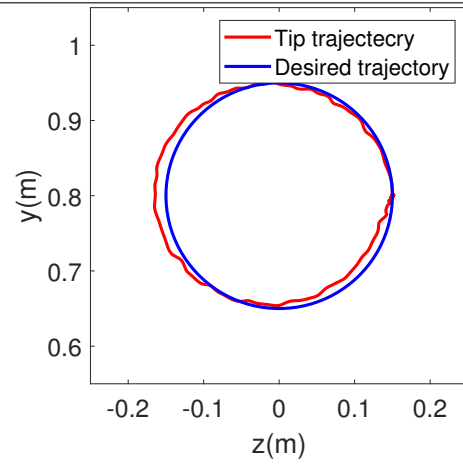

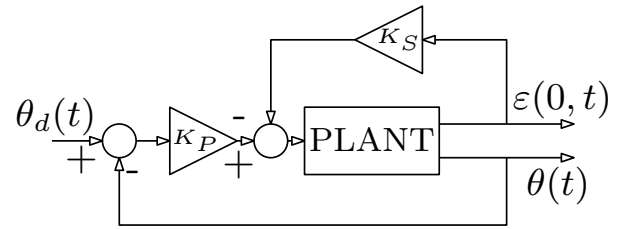**Fig. 3.** Tip trajectory of kinematic model

Fig. 4. P controller and strain feedback

FFT analysis in the x, y, and z confirmed the resonance frequency to be around 3Hz in all axial directions.

Having obtained the tip trajectory in 3D space for the respective joint angles, system identification was performed with the joint angles as the input data and the tip trajectory as the output data. This yielded as linear state space system representing the model manipulator. With the generated state space model, we investigated various control schemes for comparison and vibration control.

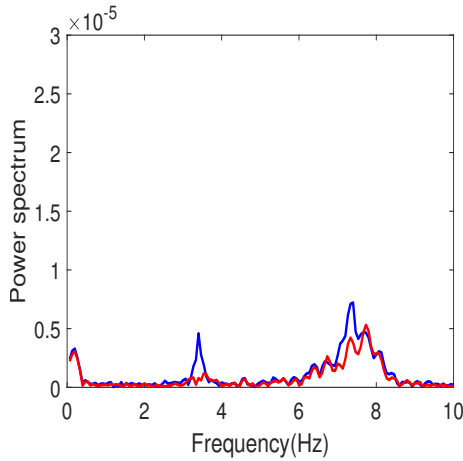## 4. State space control schemes

4.1. Feedback control

In this section, angle control using P controller based on the input angle generated by inverse kinematics was performed, and at the same time the usefulness of tip trajectory generation and vibration suppression by using direct strain feedback are verified.

Figure 4 shows a block diagram of the controller. When the angle control is performed by P control, the root strain signal $\varepsilon(0,t)$ was simultaneously multiplied by the feedback gain K_S to directly feed back to the input signal to the motor. In this experiment, the feedback gain applied to the distortion signal for the driving surfaces of Joint 2 and Joint 3 was set to 0.4 and as mentioned earlier, the proportional gain was set to 3.

Figure 5 shows the FFT of the measured value of the strain gauge of Link 1 and link 2 with and without strain feedback controller. It can be seen that the resonant frequency of the flexible manipulator is approximately 3Hz with the other peak around 7Hz. Further, it can be
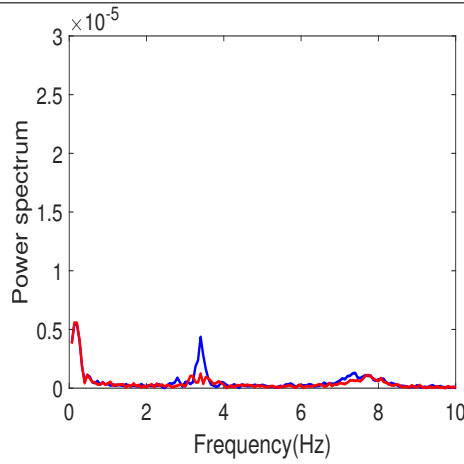
(a) FFT analysis of link 1 strain

(b) FFT analysis of link 2 strain

Fig. 5.   FFT analysis of the model

Fig. 6.   Tip trajectory with strain feedback (DSFB)

(a) Pole-Zero map of the identified model

(b) Pole-Zero map of the inverse model

Fig. 7.   Model identification results

seen that strain feedback suppress vibration both at the resonant frequency but fails to suppress higher harmonics as seen for the peak at 7Hz.From this, there is no guarantee that the vibration at the tip can be suppressed by feedback strategies alone.

Figure 6 shows the trajectory of the tip of the flexible manipulator on the yz plane. The radius error in y direction is 0.0107[m], which is larger than that of Figure 3. This is considered to be the effect of steady strain due to gravitational self-weight of the links. Since the flexible manipulator used in this study has a very low rigidity, it is always distorted due to its own weight when it is tilted to the ground. In the direct strain feedback, this steady strain amount is also fed back to the angle input, so that an angle error is generated accordingly.

In the simultaneous control of trajectory tracking by inverse kinematics and vibration control by direct strain feedback, it was confirmed that direct strain feedback was effective for removing some resonance frequency components. However, the error of the steady strain is also fed back, and the accuracy of the trajectory is degraded. In order to reduce this error, it is necessary
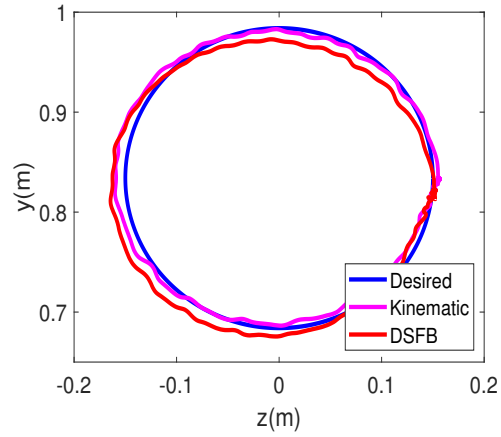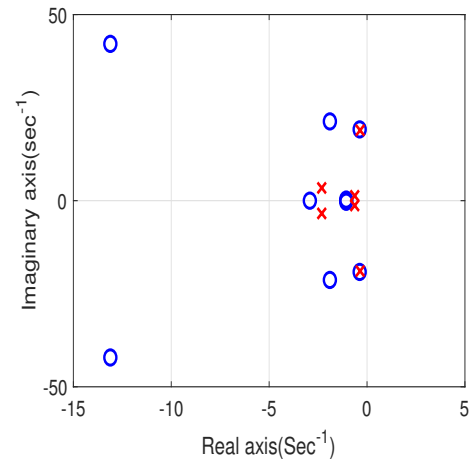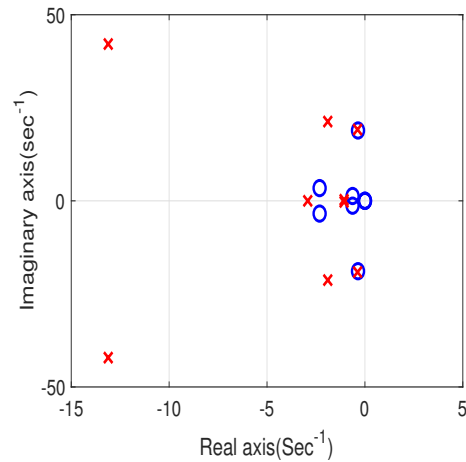
to feed back the amount obtained by subtracting the magnitude of steady strain when the manipulator was tilted. The feedback gain was again set to 0.4, but if the tip speed changed, the gain value should be adjusted accordingly. Further, the strain gauge used this time was attached at the root, but there is a delay before
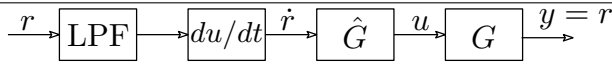
Fig. 8. Filter inverse control system

(a) Magnitude

the vibration generated at the root was transmitted to the tip. If control was not performed after taking these factors into consideration, the vibration of the tip may be worsened and the accuracy of the trajectory may be adversely affected.

In the next section, identification of the system based on the displacement of each joint and tip, rather than the root strain will be performed. Development of inverse system from the identified model, and examination of the model in vibration suppression method will be carried out.

4.2. Inverse system control

From the input and output data obtained by the inverse kinematics, system identification was performed using the canonical variate analysis method in the System Identification Toolbox of Matlab. The input data here was the displacement of each joint measured by the encoder, and the output data is the trajectory measured by OptiTrack. Since the system has multiple inputs and multiple outputs, the state space model was used and the number of states were 10. Since the direct transfer term D was set to 0, the equation of state of the identification system is expressed by equation (17) and (18).

$$\dot{x} = Ax + Bu \tag{17}$$
$$y = Cx \tag{18}$$

Where x, y and u are expressed as follows.

$$x = \begin{bmatrix} x_1 & x_2 & x_3 & x_4 & x_5 & x_6 & x_7 & x_8 & x_9 & x_{10} \end{bmatrix}^T$$
$$y = \begin{bmatrix} y_1 & y_2 & y_3 \end{bmatrix}^T$$
$$u = \begin{bmatrix} u_1 & u_2 & u_3 \end{bmatrix}^T$$

For details of these state matrices, see appendix (B).

Elements y_1, y_2 and y_3 indicate the x, y, z of the tip trajectory, and u_1, u_2, u_3 are the displacements of the input angles to Joint 1, Joint 2, and Joint 3. The inverse system was derived using the construction algorithm proposed by Silverman et al. [26] and other sources as discussed in [27], [28]. First, the lower expression of equation (18) is differentiated to derive (19).
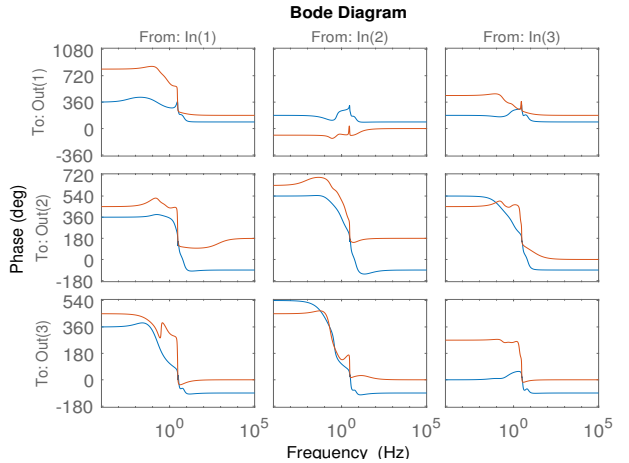
$$\dot{y} = C\dot{x} \tag{19}$$

Next, the above equation is substituted into equation (17) yielding (20).

$$\dot{y} = C\dot{x}$$
$$= CAx + CBu \tag{20}$$
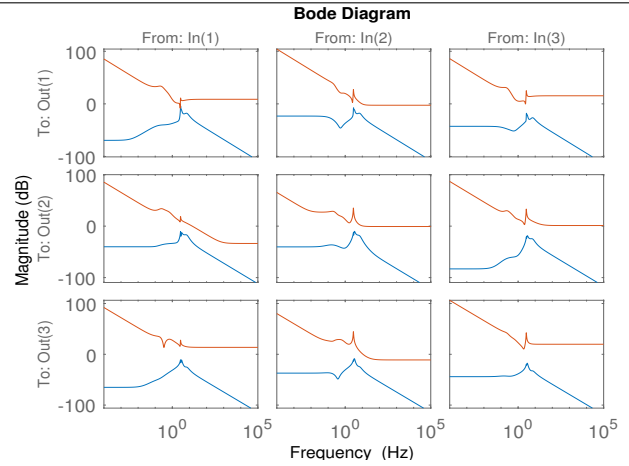
(b) Phase

Fig. 9. Bode plots of the identified and inverse system models

Then checking if $CB \neq 0$ in equation (20), when $CB = 0$, equation (20) is differentiated. Repeating this n times, when $CA^nB \neq 0$ as shown in (21).

$$y^n = CA^nx + CA^{n-1}Bu \tag{21}$$

From the above, the equation (21) is rearranged as follows.

$$u = (CA^{n-1}B)^{-1}[y^n - CA^nx] \tag{22}$$

Substituting equation (22) into (17).

$$\dot{x} = Ax + B(CA^{n-1}B)^{-1}y^n - B(CA^{n-1}B)^{-1}CA^nx$$
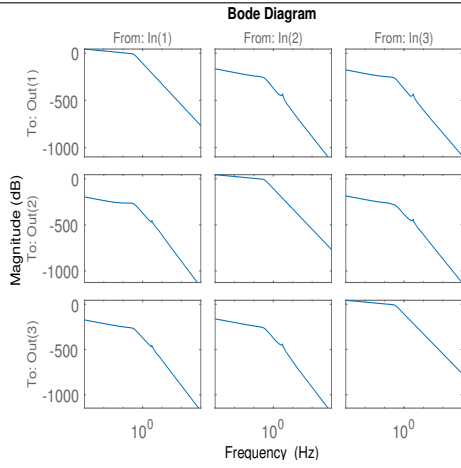$$= [A - B(CA^{n-1}B)^{-1}CA^n]x \tag{23}$$
$$+ B(CA^{n-1}B)^{-1}y^n$$

Also, from (22), u can be expressed as (24).

$$u = -(CA^{n-1}B)^{-1}CA^nx + (CA^{n-1}B)^{-1}y^n \tag{24}$$
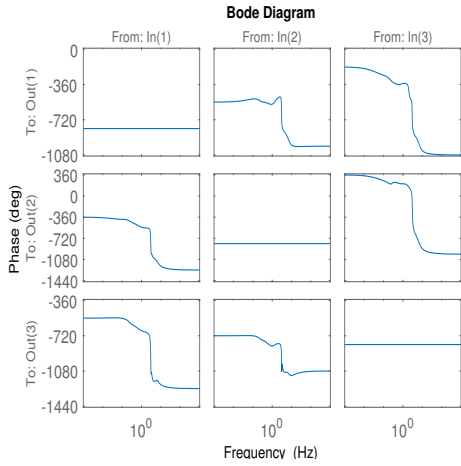
From the above, the equation of state of the inverse system is expressed by the following equation (25) and (26).

$$\dot{\hat{x}} = \hat{A}\hat{x} + \hat{B}y^n \tag{25}$$
$$u = \hat{C}\hat{x} + \hat{D}y^n \tag{26}$$

(a) Magnitude

(b) Phase

Fig. 10. Bode plots of the filtered inverse system

Fig. 11. Experimental tip trajectory

Fig. 12. FFT analysis

where:

$$\hat{A} = Ax + B(CA^{n-1}B)^{-1}$$
$$\hat{B} = B(CA^{n-1}B)^{-1}CA^n$$
$$\hat{C} = -(CA^{n-1}B)^{-1}CA^n$$
$$\hat{D} = (CA^{n-1}B)^{-1}$$

For details of these state matrices, see appendix C.

The model derived above was simulated in Matlab to verify performance. Figure 7(a) shows the pole-zero map of the identified system. Since the poles are concentrated on the left half plane, it can be seen that it is a stable system. Further, since all zeros are concentrated on the left half plane, the model is minimum phase and the resulting inverse system will be stable. Since the flexible manipulator is a non-minimum phase system, it generally has unstable zeros, however, during identification, minimum phase model that does not have unstable zeros was settled upon to evade the complexity that comes with inverting a non minimum phase model. This way, it was possible to sufficiently reproduce vibration characteristics.
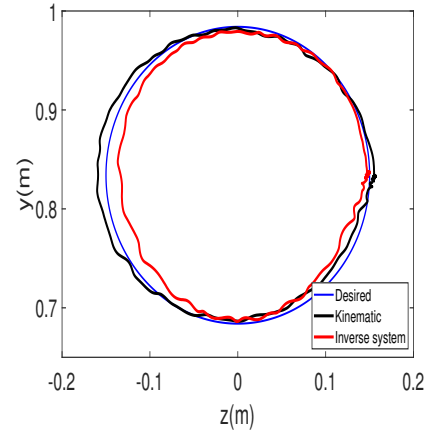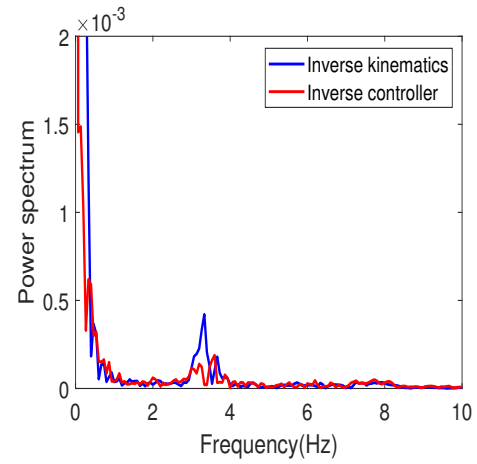
Figure 7(b) shows the pole-zero map of the inverse system. Compared with the pole-zero map of the identification system shown in Figure 7(a), it can be confirmed that the placements of poles and zeros are interchanged. As a result, the controlled object and the poles and zeros of the inverse system cancel each other out, suppressing vibration. The pole near the origin of the inverse system has a positive real part, but its value is sufficiently small that it has no adverse effect in this experiment, so it was neglected.

Having performed system identification and inverse system development, next we describe the low reproducibility of high frequency components, which is a drawback of the inverse system and the solution to it. In general, most existing physical systems have integral characteristics that attenuate high frequency components. Since the inverse system also cancels this integral characteristic, it may amplify high frequency components and adversely affect the entire system. Therefore, in this work, filtered inverse system that used a low-pass filter was employed. In this method, high-frequency components are attenuated by a low-pass filter, and only low-frequency components are reproduced as discussed in

[5]. In the study, we set the cutoff frequency of the low-pass filter to 50Hz because it is outside the 3Hz that was the resonant frequency of the manipulator system.

The proposed approach for inverse model is shown in Figure 8. Variable r is the target value and u is the input value for the target value. Variable y is the output from the system, G is the identified model, and G^{-1} is the inverse system. In this experiment, r is the target trajectory and u is the target angle of each joint.

Figure 9 shows the bode plots for the magnitudes (Figure 9a) and phase (Figure 9b) of the identified and the inverse models in the same figure. From Figure 9a, it can be seen that the magnitude plots of the inverse model resemble that plot for the identified model flipped about the resonant frequency ranges. The profile of the phase plots of the two models is also similar as can be seen in Figure 9b. The minor discrepancy between the plots of the two model stems from the unstable pole of the inverse system that was not ignored in the analysis. The differences of the inverted scheme are addressed by the filtering process as described above. After filtering, the results are as shown in Figure 10. From the figure, the frequency response is generally flat. This confirms the attenuation of high frequency component of the signals.

The developed simulation model above was deployed to the actual manipulator for verification of performance. The experimental results are as shown in Figure 11. From the figure, the radius error was reported as -0.0066[m] in z-direction and -0.0034[m] in y-direction. This is an improvement in the y-direction from the DSFB that reported an error of 0.0107[m]. Also, trajectory tracking using the inverse system reported better accuracy than using the inverse kinematics approach. This was attributed to the fact that the inverse kinematics did not consider the deflection due to the self weight of the links in the determination of the joint angles. On the other hand, the inverse system performed system identification from the actual input/output relationship, and thus considered the deflection due to its own weight.

As shown in Figure 12, the inverse controller suppressed the resonance frequency component near 3Hz, which demonstrated its effectiveness. The resonance frequency component around 7Hz was not improved. This is considered to be because the frequency response could not be reproduced well because the state variable was set low in order to create a model without unstable zeros during system identification.

5. Conclusion

In this study, we designed a controller and verified its performance by using a 2-link 3-DOF flexible manipulator to simultaneously perform trajectory control and vibration control. First, as a result of performing trajectory control using inverse kinematics, it was confirmed that the trajectory tracking performance deteriorates due to deflection due to the self weight of the links, and

that the vibration component near the resonant frequency of the flexible manipulator occurs at 3Hz. Next, the effectiveness of simultaneous control of trajectory generation by inverse kinematics and simultaneous vibration suppression method using direct strain feedback, which has been used in many studies, was verified. Further, we confirmed that direct strain feedback was effective in suppressing tip vibration. However, at the same time, we also confirmed that a large error occurs in the tip trajectory due to the effect of steady strain due to gravity. Finally, system identification was performed from the results of the control experiment by inverse kinematics, and the the state space inverse system was developed. Inverse modes become unreliable in higher frequencies. In this study, we applied a low pass filter of 50 Hz to limit the frequencies which is within the operating frequencies of the actual model.

The results of the proposed filtered inverse system is compared to the trajectory and vibration control schemes of strain feedback and kinematic model. The proposed inverse model reported tracking error 9-fold tracking improvement compared to the other two. From this, experiments on an actual machine using filtered inverse controller showed the effectiveness of controller for sufficient tracking of the ideal trajectory and suppression of resonant frequency components near 3Hz.

References

[1] K. Lochan, B. K. Roy, and B. Subudhi, "A review on two-link flexible manipulators," *Annual Reviews in Control*, vol. 42, pp. 346–367, 2016.

[2] F. Rubio, F. Valero, and C. Llopis-Albert, "A review of mobile robots: Concepts, methods, theoretical framework, and applications," *International Journal of Advanced Robotic Systems*, vol. 16, no. 2, pp. 1–22, 2019.

[3] D. K. Thomsen, R. Søe-Knudsen, O. Balling, and X. Zhang, "Vibration control of industrial robot arms by multi-mode time-varying input shaping," *Mechanism and Machine Theory*, vol. 155, p. 104072, 2021.

[4] L. Ben Tarla, M. Bakhti, and B. Bououlid Idrissi, "Implementation of second order sliding mode disturbance observer for a one-link flexible manipulator using Dspace Ds1104," *SN Applied Sciences*, vol. 2, no. 3, p. 485, 2020.

[5] W. Njeri, M. Sasaki, and K. Matsushita, "Enhanced vibration control of a multilink flexible manipulator using filtered inverse controller," *ROBOMECH Journal*, vol. 5, no. 1, p. 28, 2018.

[6] A. De Luca, "Trajectory control of flexible manipulators BT - Control Problems in Robotics and Automation," (Berlin, Heidelberg), pp. 83–104, Springer Berlin Heidelberg, 1998.

[7] M. A. Ali, F. B. Ismail, K. Sahari, K. Weria, Y. Moslem, R. Izaizi, and M. Abdollahian, "Trajectory Tracking Controller for flexible robot arm," *2014 IEEE International Symposium on Robotics and Manufacturing Automation, IEEE-ROMA2014*, pp. 39–45, 2015.

[8] D. Pavlichenko and S. Behnke, "Flexible-Joint Manipulator Trajectory Tracking with Learned Two-Stage Model employing

One-Step Future Prediction," pp. 1–9, 2022.

[9] L. Tang, M. Gouttefarde, H. Sun, L. Yin, and C. Zhou, "Dynamic modelling and vibration suppression of a single-link flexible manipulator with two cables," *Mechanism and Machine Theory*, vol. 162, p. 104347, 2021.

[10] Yavuz, L. Malgaca, and H. Karagülle, "Vibration control of a single-link flexible composite manipulator," *Composite Structures*, vol. 140, pp. 684–691, 2016.

[11] Z. Luo, F. Matsuno, and Y. Sakawa, "Experimental Study on Feedback Control of Coupled Bending and Torsional Vibrations of Flexible Beams," *IFAC Proceedings Volumes*, vol. 22, no. 4, pp. 327–332, 1989.

[12] Z. H. Luo, "Direct strain feedback control of flexible robot arms: new theoretical and experimental results," *IEEE Transactions on Automatic Control*, vol. 38, no. 11, pp. 1610–1622, 1993.

[13] Z.-H. Luo and Y. Sakawa, "Gain adaptive direct strain feedback control of flexible robot arms," in *Proceedings of TENCON '93. IEEE Region 10 International Conference on Computers, Communications and Automation*, vol. 4, pp. 199–202 vol.4, 1993.

[14] W. Njeri, M. Sasaki, and K. Matsushita, "Gain tuning for high-speed vibration control of a multilink flexible manipulator using artificial neural network," *Journal of Vibration and Acoustics, Transactions of the ASME*, vol. 141, no. 4, 2019.

[15] M. Sasaki, A. Asai, T. Shimizu, and S. Ito, *Self-tuning control of a two-link flexible manipulator using neural networks*. sep 2009.

[16] S. S. Ge, T. H. Lee, and G. Zhu, "Energy-based robust controller design for multi-link flexible robots," *Mechatronics*, vol. 6, no. 7, pp. 779–798, 1996.

[17] S. S. Ge, T. H. Lee, and Z. P. Wang, "Adaptive robust controller design for multi-link flexible robots," in *Proceedings of the 2001 American Control Conference. (Cat. No.01CH37148)*, vol. 2, pp. 947–952 vol.2, 2001.

[18] M. M. İlman, Yavuz, and P. Y. Taser, "Generalized Input Preshaping Vibration Control Approach for Multi-Link Flexible Manipulators using Machine Intelligence," *Mechatronics*, vol. 82, p. 102735, 2022.

[19] M. J. Mahmoodabadi and N. Nejadkourki, "Trajectory Tracking of a Flexible Robot Manipulator by a New Optimized Fuzzy Adaptive Sliding Mode-Based Feedback Linearization Controller," *Journal of Robotics*, vol. 2020, 2020.

[20] L. Cui, H. Wang, and W. Chen, "Trajectory planning of a spatial flexible manipulator for vibration suppression," *Robotics and Autonomous Systems*, vol. 123, p. 103316, 2020.

[21] M. Uchiyama, "Trajectory Control of Flexible Manipulators.," *Journal of the Robotics Society of Japan*, vol. 12, no. 2, pp. 184–191, 1994.

[22] F. Zhang and Z. Yuan, "The study of dynamic modeling and multivariable feedback control for flexible manipulators with friction effect and terminal load," *Sensors*, vol. 21, no. 4, pp. 1–18, 2021.

[23] W. E. Abdul-Lateef, A. F. Huayier, and N. H. Farhood, "Design of planning trajectory for the planar robot manipulator using linear segments method with parabolic blends (LSPB)," *Journal of Mechanical Engineering Research and Developments*, vol. 44, no. 3, pp. 159–171, 2021.

[24] D. Joo and K. Yeom, "Improved Hybrid Trajectory Tracking Algorithm for a 3-link Manipulator Using Artificial Neural Network and Kalman Filter," *International Journal of Mechanical Engineering and Robotics Research*, vol. 10, no. 2, pp. 60–66, 2021.

[25] N. Mishra and S. P. Singh, "Determination of modes of vibration for accurate modelling of the flexibility effects on dynamics of a two link flexible manipulator," *International Journal of Non-Linear Mechanics*, vol. 141, no. August 2021, p. 103943, 2022.

[26] L. Silverman, "Inversion of multivariable linear systems," *IEEE Transactions on Automatic Control*, vol. 14, no. 3, pp. 270–276, 1969.

[27] J. Descusse, "State feedback decoupling with stability of linear constant (<tex>A,B,C,D</tex>) quadruples," *IEEE Transactions on Automatic Control*, vol. 25, no. 4, pp. 739–743, 1980.

[28] Y. Jung, *Inverse system identification with applications in predistortion*. 01 2019.

Appendix

Appendix A
Transformation matrix

$$
{}^0T_3 = \begin{bmatrix}
\cos\theta_1\cos(\theta_2+\theta_3) & -\cos\theta_1\sin(\theta_2+\theta_3) & -\sin\theta_1 & \cos\theta_1(l_1\cos\theta_2+l_2\cos(\theta_2+\theta_3)) \\
\sin\theta_1\cos(\theta_2+\theta_3) & -\sin\theta_1\sin(\theta_2+\theta_3) & 0 & \sin\theta_1(l_1\cos\theta_2+l_2\cos(\theta_2+\theta_3)) \\
\sin(\theta_2+\theta_3) & \cos(\theta_2+\theta_3) & 0 & l_1\sin\theta_2+l_2\sin(\theta_2+\theta_3)) \\
0 & 0 & 0 & 1
\end{bmatrix}
$$

Appendix B
State space matrices of the identified model

$$
A = \begin{bmatrix}
-0.6926 & -0.8675 & 0.0516 & -0.0511 & 0.2786 & 0.5353 & -0.1166 & 0.1086 & -0.1400 & 0.4740 \\
0.4900 & -1.5583 & -0.5355 & 0.0367 & -0.8306 & 0.2203 & -1.5467 & -0.0287 & -1.1216 & 2.0692 \\
-0.1760 & 3.5986 & -3.2778 & 1.9900 & -6.8039 & -3.7085 & -4.7814 & -1.4837 & -2.0616 & 1.3883 \\
-0.0582 & 0.1535 & -2.6397 & -3.5329 & -0.3705 & 1.3518 & -3.8494 & 6.5161 & -3.3288 & 11.8725 \\
-0.1508 & 2.4174 & 7.2666 & -2.4489 & -0.3628 & -10.9042 & 10.2229 & 4.6523 & 4.2277 & 0.0171 \\
-1.0621 & 0.1789 & 7.7042 & -9.7875 & 5.0168 & 3.3471 & 9.5343 & -1.6831 & -4.3811 & 9.8268 \\
0.6934 & 2.1370 & 11.7847 & 2.8564 & -17.6533 & -0.1577 & 2.4951 & -3.9490 & 3.4115 & 2.2134 \\
-2.6478 & -0.4796 & 34.4820 & -64.7539 & -43.5529 & 27.7574 & 13.5589 & 6.4922 & 32.2565 & 18.0729 \\
2.6061 & 10.8855 & 16.4387 & 18.3434 & -24.6379 & 33.9769 & 8.8472 & -40.4746 & -25.6975 & -43.7943 \\
0.9775 & -0.2089 & 2.8948 & -14.2132 & -4.8481 & 0.2834 & -6.0791 & 16.9463 & -6.6456 & -28.3385
\end{bmatrix}
$$

$$
B = \begin{bmatrix}
-1.0210 & -0.5904 & -0.5717 \\
5.2493 & 6.9163 & 1.8214 \\
32.5313 & 32.2858 & 13.8965 \\
-59.0933 & -36.6227 & -29.2562 \\
-78.8517 & -78.9634 & -28.0289 \\
-0.6712 & -5.8014 & 1.7168 \\
48.7067 & 34.2729 & 22.7535 \\
-298.4638 & -412.3211 & -42.6761 \\
538.8148 & 504.9310 & 184.5226 \\
218.7773 & 210.5332 & 78.9056
\end{bmatrix}
$$

$$
C = \begin{bmatrix}
0.7545 & -0.0670 & -0.0168 & 0.0051 & 0.0053 & 0.0075 & 0.0048 & 0.0004 & 0.0331 & 0.0004 \\
-0.2734 & -0.0851 & -0.0167 & -0.0591 & -0.0091 & -0.0016 & 0.0046 & -0.0032 & -0.0026 & -0.0079 \\
0.8109 & 0.1275 & 0.0503 & -0.0297 & -0.0123 & 0.00048 & 0.0013 & 0.0004 & -0.0051 & -0.0008
\end{bmatrix}
$$

$$
D = \begin{bmatrix}
0 & 0 & 0 \\
0 & 0 & 0 \\
0 & 0 & 0
\end{bmatrix}
$$

Appendix C
State space matrices of the inverse model

$$
\hat{A} = \begin{bmatrix}
-0.7498 & -0.9482 & -0.0126 & 0.1634 & 0.3362 & 0.4609 & -0.1429 & 0.0101 & -0.0672 & 0.3618 \\
-4.9467 & -9.6075 & 1.23210 & 0.0750 & 2.8272 & 5.1341 & -0.7792 & -0.0170 & -1.2179 & 4.4401 \\
-21.6027 & -28.2769 & 3.85970 & -1.0576 & 6.0569 & 16.9038 & -2.9337 & 0.0051 & -4.1027 & 14.1147 \\
24.1976 & 36.9731 & 7.98470 & 9.4114 & 6.4490 & 23.7448 & 2.6950 & 0.6424 & 5.6125 & 16.6298 \\
94.5975 & 144.7693 & -11.5565 & 6.9109 & -44.3194 & -92.9686 & 20.3899 & 0.2904 & 17.6722 & -67.5642
\end{bmatrix}
$$

$$
\hat{B} = \begin{bmatrix}
0.0415 & -0.3757 & -0.2624 \\
-5.6923 & -1.9402 & -5.1393 \\
-22.4575 & -1.5935 & -18.4455 \\
20.9541 & -18.4306 & 19.4764 \\
81.7583 & 6.0869 & 99.2044 \\
10.2468 & 5.3027 & 14.0964 \\
-23.9267 & 11.0621 & -24.6789 \\
618.1098 & 144.7863 & 865.8609 \\
-591.7940 & -11.7588 & -786.0879 \\
-221.1660 & -8.7231 & -273.9078
\end{bmatrix}
$$

$$
\hat{C} = \begin{bmatrix}
-4.6568 & -7.0624 & 0.0167 & -0.6707 & 0.9621 & 3.5661 & -2.0358 & 0.2826 & -1.2520 & 4.6948 \\
0.7303 & 1.1503 & 0.3038 & 0.4092 & 0.3815 & -0.4850 & 0.9429 & -0.1721 & 0.5233 & -1.4615 \\
7.6627 & 11.5665 & -0.2313 & 0.4000 & -2.2131 & -5.7380 & 2.7079 & -0.1547 & 1.5681 & -6.6791
\end{bmatrix}
$$

$$
\hat{D} = \begin{bmatrix}
-2.7328 & 0.7425 & -5.8814 \\
-0.0208 & -0.9175 & 1.1451 \\
4.8297 & 0.2787 & 9.7806
\end{bmatrix}
$$